IEEE Access
Multidisciplinary | Rapid Review | Open Access Journal

Received 8 August 2023, accepted 28 August 2023, date of publication 6 September 2023, date of current version 5 October 2023.

Digital Object Identifier 10.1109/ACCESS.2023.3312616

RESEARCH ARTICLE

Nuclear Cataract Database for Biomedical and Machine Learning Applications

ISRAEL CRUZ-VEGA, HANS ISRAEL MORALES-LOPEZ, JUAN MANUEL RAMIREZ-CORTES, (Senior Member, IEEE), AND JOSE DE JESUS RANGEL-MAGDALENO, (Senior Member, IEEE)
Department of Electronics, National Institute of Astrophysics, Optics and Electronics, Puebla 72840, Mexico
Corresponding author: Israel Cruz-Vega (icruzv@inaoep.mx)

ABSTRACT A cataract is a medical condition causing an opacity in the ocular nucleus due to various factors such as age and diseases. Starting from traditional image processing techniques for processing and extracting relevant features, using computational intelligence methods is essential to help experts in the medical pre-diagnosis for automatic classification and grading of the disease. However, the learning capabilities of such automated processes rely considerably upon the availability of adequately-labeled databases approved by medical experts. Considering the shortage of available public databases for implementing potential algorithms such as Deep Learning, this work presents a new nuclear cataract database composed of 1437 labeled images for multi-level classification according to the LOCS III system. The images were obtained and correctly classified by experts from an ophthalmologic medical center in Mexico City. Also, our research compares relevant Machine Learning algorithms employed for medical images like Support Vector Machines, Deep Learning structures like GoogLeNet, and our proposed Deep Learning Structure with the highest classification rates for the two and multiple cataract levels according to LOCS III.

INDEX TERMS Nuclear cataract classification, machine learning, deep learning.

I. INTRODUCTION

Machine learning (ML) is transforming the practice of medicine. ML applications comprehend a series of techniques helping doctors diagnose patients more accurately, predict their future health, and recommend better treatments [1]. ML is not just a new tool but a fundamental technology required to meaningful process data exceeding the capacity of the human brain to comprehend [2]. However, ML requires a sufficient quantity and quality of data in the learning process to obtain the highest levels of accuracy [3], [4]. In this work, we present the results of our work in the recollection of nuclear cataract images, an opacity or cloud developed in the eye nucleus.

First, formally describing this eye affectation, a cataract is a medical condition causing an opacity in the region of the ocular nucleus due to various factors (in order of importance): age, diabetes, congenital formation, or eye trauma [5]. Fibrosis occurs in the ocular nucleus, causing lens hardening due to any of the factors mentioned above [6].

The World Health Organization (WHO) estimated at least 2200 million people with visual impairment or blindness in 2020, from where 1000 million have a moderate or severe deficiency that could be prevented and treated. Approximately 65.2 million worldwide suffer from cataracts due to senile degeneration [7]. Some factors causing this disease, especially at an earlier age, include the lack of ophthalmologists, specialized medical facilities, and a lack of adequate medical equipment [8].

Regular eye exams prevent vision loss due to age-related factors or a medical condition that causes eye disease. The most common test is the slit lamp examination, allowing the ophthalmologist to obtain information within the ocular

The associate editor coordinating the review of this manuscript and approving it for publication was Tao Huang.

lens detecting anomalies such as retinopathy, glaucoma, or cataracts [8]. When the cataract is within an advanced stage, requiring the surgical replacement of the ocular lens, an ultrasound examination determines the characteristics of the intraocular lens offering better features to restore the patient's vision [9].

The primary purpose of this paper is to present a new database of nuclear cataracts and make it freely available to the public. This database was obtained during our research at the Conde Valenciana Institute in Mexico City, consulting medical specialists to obtain the images with the proper medical protocol and in the subsequent validation and labeling. The database contains two cases in general: images of patients with nuclear cataracts and disease-free patients (called binary classes). The other case is a database with the multiple-degree disease levels, aimed to be compared with the LOCS III system [10]. Another purpose of the paper is to implement relevant ML classification techniques like Deep Learning and Support Vector Machines (SVM), first employing standard transfer learning DL structures like GoogLeNET and then proposing our DL structure called NCC-net (Nuclear Cataract Classification Network) aiming to obtain the best classification results for binary and multiple-levels of the disease.

After the introduction, the paper's structure includes the following sections: Section (II) mentions the state of the art of the existing databases of nuclear cataracts, and States of the art of methods for pre-processing, segmentation, and classification. The following Section (III) details the characteristics of the slit-lamp, the medical protocol followed to obtain the images, and the dataset's characteristics. Section (IV) presents the results of applying the computational intelligence classifiers like Support Vector Machines (SVM) and Deep Learning (DL). The experiments comprise the two-classes or binary classification and the multiple-level degree classification. The experimental work also includes an implementation of our proposed NCC-net on a Raspberry Pi. Finally, Section (V) contains the conclusions.

II. STATE OF THE ART

A. DATA BASES

Cataracts are classified depending on the involved area and graded by comparing the image obtained in the biomicroscopy exam with a collection of standard images labeled with the progression degree of the disease [11]. Two types of well-standardized classification systems are The Oxford Clinical Cataract Classification and Grading System (OCCCGS) [12] and Lens Opacities Classification System III (LOCS III) [13].

In the literature, six image types constitute the base for cataract classification/grading: slit lamp image, retro illumination image, ultrasonic image, fundus image, digital camera image, and anterior segment optical coherence tomography. The existing cataract classification/grading systems are based on slit and fundus images, the most commonly used ophthalmic images for clinical diagnosis and scientific research [14].

We identified some research works based on slit lamp images; these works and the number of samples used are mentioned in Table 1. Next mentioned the public and private datasets:

Private Datasets

1) **ACHIKO-NC** dataset contains slit lamp images selected from the Singapore Malay Eye Study (SiMES I) database and is comprised of 5378 images with decimal grading score (0.3 to 5.0) [15].
2) **ACHIKO-Retro** dataset contains retro-illumination lens images selected from the SiMES I dataset and is used to grade CC and PSC [16].
3) **CC Cruiser** dataset contains 476 normal and 410 cataract infantile slit-lamp images collected from the Zhongshan Ophthalmic Center of Sun Yat-Sen University, China [17].
4) **Multicenter** dataset contains 336 normal and 421 infantile cataract slit-lamp images; this dataset again comes from Asia and is collected from four clinical institutions: the central hospital of Wuhan, Shenzhen eye hospital, Kaifeng eye hospital, and the second affiliated hospital of Fujian medical university, from China [17].

Public Datasets

1) **EyePACS** dataset is a platform for retinopathy screening from the California Healthcare Foundation (http://www.eyepacs.com, https://www.kaggle.com/c/diabetic-retinopathy-detection), and is comprised of 88702 fundus retinal images [18].
2) **HRF** dataset is the high-resolution Fundus (HRF) image dataset selected from different open-access datasets: structured analysis of the retina (STARE) [19], standard diabetic retinopathy database (DIARETDB0) [20], methods to evaluate segmentation and indexing techniques in the field of retinal ophthalmology (MESSIDOR) database [21], digital retinal images for vessel extraction (DRIVE) database [22], digital retinal images for optic nerve segmentation database (DRIONSDB) [23], Indian diabetic retinopathy image dataset (IDRiD) [24], and other Internet sources.

Comments

After mentioning some of the databases found in the literature, some concerns are:

- Many databases are private and unavailable for academic purposes and research.
- Actually, many automatic diagnosis systems are based on Deep Learning, providing a high level of accuracy for classification, grading, and segmentation, among other tasks. However, these algorithms mainly require vast data for the learning process. Then it is necessary to create database repositories available for the scientific

community to train all these massive-structure algorithms.
- In the literature, many databases are mentioned from Asia countries, as shown in Table 1. Still, it is necessary to count for databases from Latin American countries where we can find other relevant features for determining eye diseases.

B. PRE-PROCESSING AND SEGMENTATION METHODS FOR FEATURE EXTRACTION

This subsection presents some relevant pre-processing and feature segmentation methodologies to obtain the region of interest (ROI), an appropriate step before the biomedical images' feature extraction and classification.

In the pre-processing step of the obtained images, all the unnecessary information from the image is removed, preparing it for further steps. Pre-processing operations can range from simple (like a resize) to more complex (like a spatial filter). The most significant contributions in cataract image pre-processing can be observed in [25], [26], [27], and [28]. The next step is the extraction of discriminant features from the image. This step is crucial and highly dependent on the first. The high accuracy in the classification process depends on the characteristics extracted in this step, correlating each characteristic and the corresponding label [29]. The literature contains vast image processing techniques and machine learning algorithms for these two steps. Some relevant works are mentioned next.

Li et al. at [30] present a feature extraction approach where the region of interest (ROI) is obtained using an elliptical lens estimate with vertical and horizontal profile clustering and thresholding. The contour of the lens was obtained with an active shape model (ASM) using 24 contour points. This approach also uses Principal Component Analysis (PCA) to obtain the mathematical expression of the contour and use it in new images. In [31], Salla et al. use a fuzzy inference system for image-preprocessing operations separating the ROIs proposing only four rules to differentiate nuclear from cortical cataracts. In [32], the authors implement histogram equalization for pre-processing to increase the image range and assign new values to the input image pixels, aiming to obtain a flat and uniform distribution of the image histogram. Finally, the lens centroid is obtained with fuzzy K-means clustering algorithms for optical images to detect the features specific to three classes classified by Artificial Neural Networks. Yang uses fundus images and pre-processes these on the green channel of the RGB color space, arguing the best contrast between the background and the blood vessels in this channel [34]. Also, they use a top-bottom hat transformation and a tri-lateral filter to accentuate the contrast. Finally, the 24 features from 4 angles are extracted from the resulting gray-level co-occurrence matrix (GLCM). Gao et al. [35] introduce an automated system for learning slit lamp imaging characteristics and grading nuclear cataracts. Through patches, local filters are developed for each class, introduced into a convolutional network, and subsequently into a set of recurring networks to extract high-order features. Following a supervised learning strategy, the label information is the grading category of each training image. Reference [36] performs image pre-processing, extracting characteristics from fundus images. In fundus images without a cataract, structures such as vessels, blood, and the optic disc are visible, whereas in cataract images, they are not. For this purpose, the author uses the discrete wavelet transform (DWT) and the discrete cosine transform (DCT) to extract localized features related to high-frequency components and then isolate the major components for each condition. A method to evaluate blurriness for cataract diagnosis in retinal images with vitreous opacity is proposed in [37]. The lesions affecting the retinal structures are detected and removed with image segmentation by a morphological technique, avoiding erroneous detection of vitreous opacity. The features extracted are the number of pixels of the visible structures, the average contrast between the blood vessels and the background, and the local standard deviation. Xu employs a deep convolutional architecture to extract and learn discriminant features from the input image [38]. Another significant contribution is using a deconvolution network (DN) to observe how the convolutional network characterizes the cataract in each layer.

Recent works bet on using only deep learning structures, including the conventional rearranging, pre-processing, and augmentation of previous steps for feature extraction into the network. Junayed et al. [39] propose a lightweight deep structure called *CataractNet* for fundus images, obtaining competitive accuracy performance, among other measures, compared with well-known deep structures for image classification like MobileNet, VGG-16, VGG-19, Inception-v3, and ResNet-50. However, CataractNet only detects cataracts and does not grade or find the exact location of the affectation. A similar work avoids the traditional manual feature extraction and only uses a deep structure called VGG19-net, presented in [40]. Again in [41] Hoosain et al. present only a cataract detection deep convolutional neural network (DCNN) based on Res-Net50, detecting cataract and non-cataract cases of fundus images.

Generally, a tendency is observed to employ DL-structures with lightweight structures (MobileNet) for applications on embedded systems and to propose more deep structures while reducing the computational costs like the Inception networks or to increase the computational accuracy as the ResNets perform.

C. CLASSIFIERS

As a final step for every automatic grading and classification system, the classification is done according to the extracted features. In many classification systems, it is customary to use various computational intelligence techniques, but it is not always necessary [42], [43], [44], [45].

TABLE 1. Description of nuclear cataract classification systems.

Author / Year	Extracted Features	Classifier	Number of Samples	Image Size	Type of Image	Precission
Li et al. (2008) [55]	0	Area Calculation	607	640 × 480	RGB	98.2%
Li et al. (2008) [56]	0	Region Growin	611	640 × 480	RGB	98.2%
Li et al. (2008) [57]	6	SVM	1000	1536 × 2048	RGB	N/R
Li et al. (2009) [58]	21	SVM	5820	1536 × 2048	RGB	N/R
Li et al. (2008) [30]	6	SVM	3000	1536 × 2048	RGB	89.3%
Huang et al. (2009) [46]	6	Ranking	1000	2048 × 1536	RGB	N/R
Acharya et al. (2010) [32]	18	Neural Network	140	128 × 128	RGB	90%
Li et al. (2010) [59]	5	Simple Rule Based Approach	441	640 × 400	Grayscale	N/R
Li et al. (2010) [29]	21	SVM	5850	1536 × 2048	RGB	95%
Salla et al. (2010) [31]	3	Fuzzy Inference System		175 × 175	RGB	76%
Huang et al. (2011) [33]	6	Ranking	1000	2048 × 1536	RGB	N/R
Gao et al. (2011) [60]		Linear Discriminant Analysis	4545		Grayscale	84.8%
Gao et al. (2015) [35]	18	Deep Learning	5378	3048 × 2432	RGB	N/R
Song et al. (2016) [61]	83	Bayesian Network and Decision Tree	5378	3048 × 2432	RGB	N/R
Morales-Lopez et al. (2018b) [62]	6	MLP and SVM	40	1028 × 640	RGB	80%
Zhang et al. (2019) [50]	N/R	SVM and FCNN	1352	N/R	RGB	94%
Jun et al. (2019) [54]	N/R	Ranking CNN	294	N/R	RGB	95%
Hu et al. (2020) [63]	4	Yolo V3-ShuffleNet(DL)-SVM	16103	416 × 416	RGB	93.4%
Tasit et al. (2022) [64]	5	Random Forest	300	256 × 256	RGB	97.92%

The authors in [30] investigate two approaches for classifying senile cataract disease for nuclear and cortical cataracts. After using post-processing techniques removing noise with spatial filters realize only the graduation of cortical cataracts and the detection of nuclear ones. The cortical cataract is graded on backlight images, and an SVM regression calculates the degree of involvement for this condition. Reference [46] propose a nuclear cataract diagnosis system via ranking. This approximation uses a direct optimization algorithm to learn all ranking functions, presenting a list of slit-lamp images of the learned ranking functions. This work offers a new evaluation measure for learning the optimal ranking function via direct optimization. Reference [29] presents an algorithm for automatically diagnosing nuclear cataracts. The ROI is detected and segmented using an active shape model (ASM) with anatomical landmark points, extracting relevant features, and classified by an SVM. Reference [31] investigate a Fuzzy Inference System to solve the cataract detection and classification problem with minimum human interaction. The system uses trapezoidal membership functions with four parameters and fuzzy rules formulated from thresholds in the RGB image. Reference [34] automatically classifies cataracts in retinal images using an artificial neural network presenting four classes: normal, mild, moderate, or severe. The extracted features are luminescence and texture. Reference [37] shows a method to evaluate blurriness for cataract diagnosis in retinal images with vitreous opacity removal. Using a morphological technique, lesions that can modify retinal structures are detected and removed from the image avoiding erroneous detection of vitreous opacity; finally, a decision tree is constructed and trained with five grades. Reference [50] propose a six-level cataract grading method focused on the multi-feature fusion based on stacking. There are extracted two kinds of features; high-level features extracted from the residual network (ResNet18). The framework uses two support vector machine (SVM) classifiers as base learners to obtain each fundus image's probability outputs. Also, a fully connected neural network (FCNN) is used as a meta-learner to work the final classification result. Reference [54] present a ranking CNN to solve the ordinal dataset problem with non-linearity patterns between the label and features like the cataract dataset. However, due to the data imbalance, the cataract dataset performed terribly in classifying severe and typical cases. The authors try to alleviate this drawback by proposing a tournament structure instead of simply aggregating binary results.

As a final comment, experiments are difficult to recreate due to technical differences in databases and varying parameters like the number of classes between different research groups. The closest efforts of this research work are with the groups formed by [29] and [50], the latter the closest due to automatic feature extraction and multiclass classification. The main contributions in nuclear cataract classification are summarized in Table 1.

III. EXPERIMENTAL PROTOCOL DESCRIPTION

This section describes the instrument for the data acquisition, the medical protocol, a brief description of the LOCS III system, the dataset description, and the data augmentation process as a regular process used in machine learning to robustify the algorithms, making them invariant to translations, viewpoints, and others. The database was obtained from the Conde Valenciana Institute, an ophthalmologist center in Mexico City.

A. THE SLIT-LAMP

The slit lamp, indispensable for the detailed examination of eye tissues, is an essential tool in any analysis of the anterior segment, including the anterior vitreous and those structures anterior to it. The slit-lamp is sufficient to observe most

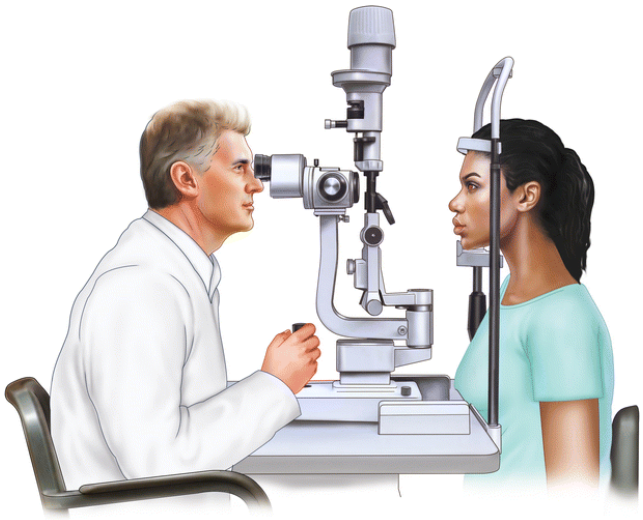

FIGURE 1. The slit lamp [51].

of the tissues in the anterior segment (except the anterior chamber angle and the posterior surface of the iris) without needing any other instrument or accessory. Fig. 1 illustrates a typical slit-lamp and the process of obtaining the images by the experts [51]. This biomicroscope consists of three main parts: The viewing arm, the illumination arm, and the patient-positioning frame.

Depending on the lighting technique used for each case, the slit lamp is used to diagnose different eye conditions. In addition, the examiner must be familiar with the lighting techniques such as diffuse illumination, direct focal illumination, specular reflection, retro illumination, indirect lateral illumination, and sclerotic scatter. Apart from the techniques mentioned above, the examiner must be familiar with the slit lamp controls that allow observing specific tissues or conditions only visible at particular inclinations of the light beam. In the case of **Diffuse illumination**, this type is commonly used to observe a general panorama of the ocular surface and intraocular structures, such as the lens, iris, nucleus, and posterior capsule. More detailed information in the use of this medical device and techniques can be found in [51].

B. THE MEDICAL PROTOCOL

To begin the test, the examiner instructs the patient to place their face firmly between the chin rest and the forehead strap. The patient's eye must be at the level of the mark on one of the support rods and below the forehead strap. The examiner must ensure that the chin is resting entirely on the chin rest and the forehead is pressing the forehead strap. The examiner must ensure the correctness of the device settings and the parameters, the patient's comfort, the normal operation of the computer interface, and the proper slit lamp distance to the eyepieces before starting the test.

Frequently, in some cataracts and mainly in senile ones, lighter and darker areas can be seen from front to back

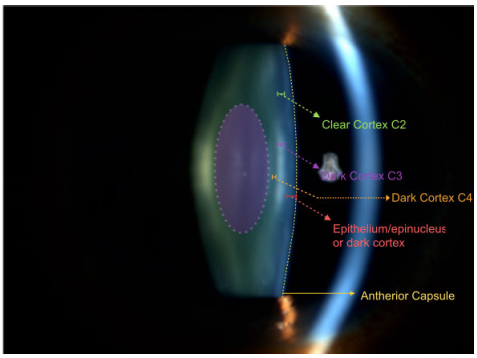

FIGURE 2. Layers of the lens cortex.

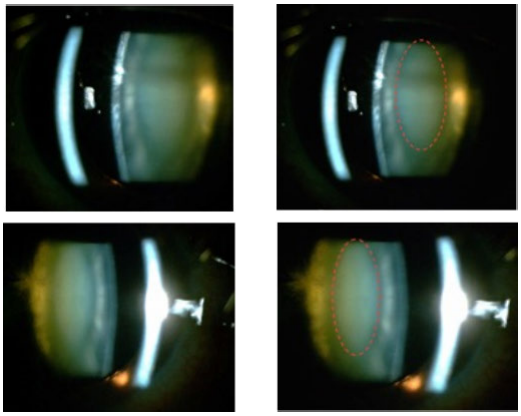

FIGURE 3. Nucleus area delimitation. (Left: Original image; Right: Lens nucleus from the original images.)

(that is, from the capsule to the nucleus). These areas are portions of transition between different layers or zones of the cortex, as seen in Fig. 2. The oval shape characterizes the nucleus, generally with the same density. Still, other transition zones are presented between the last zone of the anterior cortex and the posterior nucleus, as well as transitions through the layers forming the embryonic and fetal nucleus, as seen in Fig. 2. This approach takes a photograph when the examiner distinguishes the nucleus area from the rest of the image, as seen in Fig. 3.

C. THE LOCS III SYSTEM

The third version of the Lens Opacity Classification System (LOCS III) is a standardized system for the graduation of cataract characteristics according to age, which is highly employed and scientifically validated. LOCS III is used to graduate the cataract type, its severity, and its progression. The classification compares photographic patterns with different opacity grades of four characteristics: nuclear opacity, brunescent, cortical opacity, and posterior subcapsular opacity. The nuclear and brunescent opacities are classified according to six photography. The brightness of the nuclear region is called nuclear opalescence (NO), and the intensity of the brunescence is called nuclear color (NO). The cortical opacity grade is determined by comparing the cortical opacity

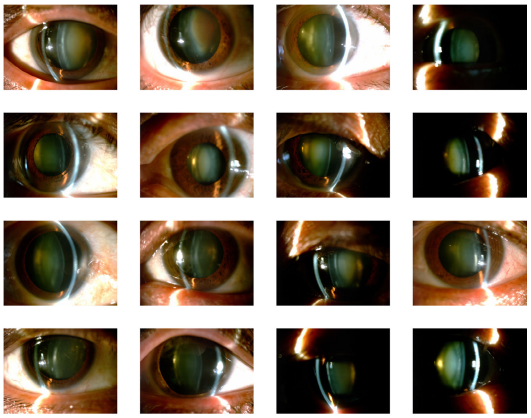

FIGURE 4. Slit-lamp dataset samples.

amount against five photography. Similarly, the subcapsular posterior opacity (P) is determined by comparing it against five other photographs showing the different opacity grades in front of the posterior capsular.

The opacity grade classification consists of identifying the patient's crystalline characteristics of the image compared to the color images. The opacity and nuclear color graduation are within a decimal scale of 0.1 to 6.9. The cortical opacity and subcapsular posterior magnitude are graduated on a decimal scale of 0.1 to 5.9. The final LOCS III classification comprehends four decimal values for NO, NC, C, and P [52].

D. THE DATASET

One of the main interests of this work is collecting slit-lamp standardized dataset images and defining the proper technical methodology. The first dataset collected consists of 40 images labeled as cataract and non-cataract. The RGB images were obtained from a Topcon DC-1 digital slit-lamp camera with a resolution of 1028 × 640 focused with a Topcon SL-D2 slit-lamp, a slit angle of 30°, a 0.5 mm aperture, and maximum luminous intensity.

The dataset collected for multi-class classification consists of 1437 labeled images. Some of these images are shown in Fig. 4. The images were obtained from a digital Topcon DC-3 slit-lamp camera with a resolution of 3264 × 2448 RGB; they were focused with a Topcon SL-D7 slit-lamp, a slit angle of 45° and 135° for each eye, a 6 mm × 0.5 mm aperture and maximum luminous intensity. The number of volunteers for the multi-class dataset was 68 women and 47 men, with at least three images per right and left eye. The expert ophthalmologists' classification according to the LOCS III Protocol is shown in Table (2. The dataset is available at Nuclear Cataract Database-DOI [53].

E. DATA AUGMENTATION

A relevant test of efficient deep network structures is the simultaneous decrease of training and validation errors.

TABLE 2. Cataract classification according to LOCS III by the expert ophthalmologists. NO: nuclear opalescence, NC: nuclear color, C: cortical, and P: posterior sub-capsular cataracts. RE: Right Eye and LE: Left Eye. IOL: intraocular lens.

Volunteer No.	Case	NO	NC	C	P	Volunteer No.	Case	NO	NC	C	P
1	RE	2	2	-	-	59	RE	3	2	-	-
	LE	1.5	1.5	-	-		LE	4.5	2	-	-
2	RE	2	3.5	-	-	60	RE	IOL	IOL	IOL	IOL
	LE	2	4.5	-	-		LE	IOL	IOL	IOL	IOL
3	RE	IOL	IOL	IOL	IOL	61	RE	-	-	-	-
	LE	4.5	5	-	-		LE	6	1.5	-	-
4	RE	4	3	-	-	62	RE	1	1	-	-
	LE	3.5	2	-	-		LE	2.5	2	-	-
5	RE	4	2	-	-	63	RE	3.5	1.5	-	-
	LE	3	3	-	-		LE	3.5	1.5	-	-
6	RE	2	3	-	-	64	RE	1	1	-	-
	LE	IOL	IOL	IOL	IOL		LE	2	2	-	-
7	RE	1.5	1.5	-	4	65	RE	2.5	2	-	-
	LE	1.5	1.5	-	3.5		LE	2.5	2.5	-	-
8	RE	-	-	-	-	66	RE	2.5	1	4	-
	LE	2	1.5	-	-		LE	2.5	2.5	4.5	-
9	RE	2.5	2	-	-	67	RE	2.5	3	-	-
	LE	2	2	-	-		LE	2.5	2	-	-
10	RE	3	4	-	-	68	RE	6	6	5	-
	LE	2.5	4	-	-		LE	3	3.5	-	-
11	RE	IOL	IOL	IOL	IOL	69	RE	1.5	1.5	-	-
	LE	4	3.5	-	-		LE	1.5	1.5	-	-
12	RE	2	2	-	-	70	RE	2	1.5	-	-
	LE	5	2	-	-		LE	2.5	2.5	-	-
13	RE	3.5	2	-	-	71	RE	2.5	2.5	5	-
	LE	3	2	-	-		LE	2.5	2.5	5	-
14	RE	IOL	IOL	IOL	IOL	72	RE	2	4	-	-
	LE	4	2.5	4	-		LE	3	5.5	-	-
15	RE	IOL	IOL	IOL	IOL	73	RE	2	2	3.5	-
	LE	IOL	IOL	IOL	IOL		LE	2	2	-	-
16	RE	3.5	2.5	-	-	74	RE	2	3.5	5	-
	LE	3	2.5	-	-		LE	3	3.5	5	-
17	RE	3.5	2.5	-	-	75	RE	3	1.5	-	-
	LE	3	3	-	2		LE	3	2.5	-	-
18	RE	2	2.5	-	-	76	RE	-	-	-	-
	LE	2	2.5	-	-		LE	3	3.5	-	-
19	RE	1.5	3.5	-	-	77	RE	2.5	5	3.5	-
	LE	1.5	3	-	-		LE	2	4	3	-
20	RE	IOL	IOL	IOL	IOL	78	RE	2.5	2	-	-
	LE	3	2	-	-		LE	-	-	-	-
21	RE	2	5	-	-	79	RE	3.5	2.5	2	-
	LE	IOL	IOL	IOL	IOL		LE	3	2	4.5	-
22	RE	IOL	IOL	IOL	IOL	80	RE	2	1.5	3.5	-
	LE	2.5	4	-	-		LE	4	4	4	-
23	RE	6	3	-	-	81	RE	2.5	2	-	-
	LE	IOL	IOL	IOL	IOL		LE	2.5	2.5	-	-
24	RE	1.5	2	-	-	82	RE	2	4	-	-
	LE	1.5	3.5	-	-		LE	6	6	-	-
25	RE	2	4.5	-	-	83	RE	3.5	2	-	-
	LE	3	2	-	-		LE	3	2	-	-
26	RE	2.5	5	-	-	84	RE	1.5	1	-	-
	LE	2.5	5	-	-		LE	-	-	-	-
27	RE	3	2	-	-	85	RE	6	2.5	-	-
	LE	3	2	-	-		LE	6	3	-	-
28	RE	IOL	IOL	IOL	IOL	86	RE	2	2	-	-
	LE	2	2.5	-	-		LE	3	3.5	-	-
29	RE	3	1.5	-	-	87	RE	5.5	5.5	-	-
	LE	2.5	1.5	-	-		LE	5	5	-	-
30	RE	IOL	IOL	IOL	IOL	88	RE	6	5	-	-
	LE	2.5	3.5	-	-		LE	6	5.5	-	-
31	RE	1.5	1.5	-	-	89	RE	2.5	2.5	-	-
	LE	1.5	1.5	-	-		LE	2	1.5	-	-
32	RE	IOL	IOL	IOL	IOL	90	RE	2.5	2.5	2.5	-
	LE	2	3.5	-	-		LE	3	3	-	-
33	RE	2.5	2	-	-	91	RE	2	2.5	-	-
	LE	3	2	3.5	-		LE	2	2	-	-
34	RE	1	1.5	-	-	92	RE	3.5	3	-	-
	LE	-	-	-	-		LE	2	2	-	-
35	RE	2	1	-	-	93	RE	3	5.5	-	-
	LE	-	-	-	-		LE	6	6	-	-
36	RE	2	3.5	4	-	94	RE	1.5	1.5	-	-
	LE	1	1.5	-	3		LE	3.5	5	-	-
37	RE	2	3.5	-	-	95	RE	4.5	4.5	-	-
	LE	IOL	IOL	IOL	IOL		LE	4	2	-	-
38	RE	2.5	2.5	-	-	96	RE	1.5	2	-	-
	LE	3	2	-	-		LE	1.5	2	-	-
39	RE	3	5	-	-	97	RE	2	2.5	-	-
	LE	blood	blood	blood	blood		LE	2.5	3	-	-
40	RE	4	3	-	-	98	RE	2	4	-	-
	LE	3	3.5	-	-		LE	2	3.5	-	-
41	RE	2	3	-	-	99	RE	2.5	1.5	-	-
	LE	2.5	3	-	-		LE	2.5	2.5	-	-
42	RE	-	-	-	-	100	RE	3	3	-	-
	LE	-	-	-	-		LE	3	3.5	-	-
43	RE	-	-	-	-	101	RE	IOL	IOL	IOL	IOL
	LE	1.5	3	-	-		LE	6	3	-	-
44	RE	2	1.5	-	-	102	RE	3	4	-	-
	LE	1.5	1.5	-	-		LE	3.5	3	-	-
45	RE	1.5	1.5	4	-	103	RE	3	3	-	-
	LE	1.5	1	-	-		LE	3.5	4	-	-
46	RE	2	3	-	-	104	RE	2	1.5	-	-
	LE	2	3	-	-		LE	1.5	1	-	-
47	RE	1.5	3.5	-	-	105	RE	6	4	-	-
	LE	1.5	3.5	-	-		LE	1.5	1.5	3.5	-
48	RE	3.5	3.5	-	-	106	RE	2	2	-	-
	LE	4	6	-	-		LE	6	3	-	-
49	RE	2.5	2.5	-	-	107	RE	1	1	4	-
	LE	2	2	-	-		LE	1	1.5	4	4
50	RE	3	3	-	-	108	RE	3	4	-	-
	LE	3	2.5	-	-		LE	5	5.5	-	-
51	RE	IOL	IOL	IOL	IOL	109	RE	1.5	3	-	-
	LE	2.5	2	4	-		LE	IOL	IOL	IOL	IOL
52	RE	IOL	IOL	IOL	IOL	110	RE	4	4	-	-
	LE	3.5	6	-	-		LE	2.5	2.5	-	-
53	RE	2	2.5	-	-	111	RE	2	2.5	-	-
	LE	3.5	3	-	-		LE	3.5	3	-	-
54	RE	3.5	2.5	-	-	112	RE	3	5	-	-
	LE	4	3	-	-		LE	3	3.5	-	-
55	RE	3.5	5.5	5	-	113	RE	3	3.5	-	-
	LE	3.5	5.5	5	-		LE	3	4	-	-
56	RE	3.5	5	-	-	114	RE	2	2.5	-	-
	LE	3.5	4.5	-	-		LE	IOL	IOL	IOL	IOL
57	RE	2.5	1	-	-	115	RE	3.5	2.5	-	-
	LE	2	1	-	-		LE	2	2	-	-
58	RE	6	6	5	-						
	LE	2.5	1	-	-						

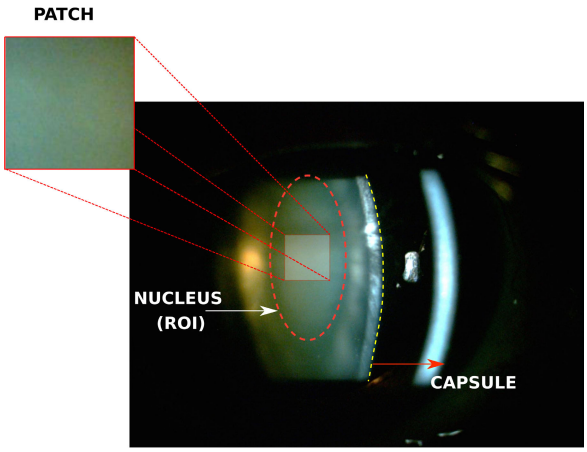

FIGURE 5. Patches from slit-lamp images.

The larger the training sets, the better the results using deep learning models. However, when it comes to medical imaging, this task is quite complicated due to the limitations and complexity of obtaining the validated databases; it is necessary for an additional process of *data augmentation*. The effectiveness of data augmentation has been proven in many cases through simple transformations, either by transforming color spaces, cropping, flipping, etc. These simple transformations can encode many variations in pattern recognition tasks. Cropping images is common in data augmentation, providing effects similar to image translation. Still, with certain differences: cropping reduces the size of the input image, while translation preserves spatial information. However, clipping the image can cause the label information to be lost, but it significantly reduces network training time due to the reduction in image dimensions.

In this work, We extracted ten patches from the ROI for each image, as shown in Fig. 5. The size of the patches is 224×224 pixels, obtaining a total of 14370 labeled images, i.e., a database augmented ten times.

IV. EXPERIMENTAL RESULTS

This section presents the main results of our work in classifying nuclear cataracts of two general cases: the binary classification and the Multiple-level case for comparisons with the LOCS III System. First, we briefly describe the machine learning-based classifiers used in this work. According to [47], Machine learning broadly refers to fitting predictive models to data or identifying informative groupings within data. ML attempts to approximate or imitate humans' ability to recognize patterns objectively using computation. The utility of ML is mainly given when the analyzed dataset is too large (many individual data points) or too complex (contains a large number of features) for human analysis and/or when the data analysis process is automated for a reproducible and time-efficient pipeline. Next, we briefly explain the two main classifiers we based our research on.

The first one is **Support Vector Machines (SVM)**, where the general idea is to provide a hyperplane to differentiate between two classes:

$$f(x) = \mathbf{w}^{\mathbf{T}}\mathbf{x} + b = 0 \tag{1}$$

where ($\mathbf{w}$ is a weight vector, and b is a bias). Unlike a classical Multilayer Perceptron, which also builds up a hyperplane as a decision surface with a neural structure, SVM maximizes the margin of separation between positive and negative examples of such classes. The solution is based on a quadratic programming problem, obtaining the optimal solution through a Lagrange formulation. When the data is nonlinear-separable, SVM uses kernel functions to construct hyperplanes in high-dimensional feature space [48].

The other classifier is based on Deep Learning (DL) [49], computational models with multiple processing layers. DL learns data representations with multiple levels of abstraction, discovering intricate structures in large datasets. This work is based on a Convolutional Neural Network (CNN), where each node is connected to only a small subset of spatially connected neurons in the input image channels; this stage is for detecting certain local features of the input channels. The kernels, which are sets of connection weights shared between the nodes, learn to detect the n local features whose strength across the input images is visible in the n resulting feature maps. Due to the high increase in parameter growth, the *pooling layer* reduces the computational complexity achieving a hierarchical set of image features. CNNs usually contain several pairs of convolutional and pooling layers, followed by several consecutive *fully connected* layers and a *softmax layer*, to generate the desired outputs. A common training algorithm is stochastic gradient descent, which minimizes the cost function:

$$L = -\frac{1}{|X|}\sum_{i}^{|X|} ln(p(y^i \mid X^i)) \tag{2}$$

where $|X|$ denotes the number of training images, X^i is the i^{th} training image with the corresponding label y^i, and $p(y^i \mid X^i)$ is the probability value indicating the correct classification of X^i.

We employ standard performance measures like sensitivity, specificity, accuracy, and the area under the curve (AUC) of the receiver operating characteristics analysis (ROC) considered as reliable evaluation metrics for classifier completeness in medical imaging [65].

This work proposes a novel network called Nuclear Cataract Classification Network (NCC-net), with the structure mentioned in Table (3).

The first dataset collected for the binary case consists of (1028 $\times$ 640-RGB) labeled images as cataract and non-cataract. The dataset collected for multi-class classification consists of 1437 labeled images obtained with the technical specifications mentioned above. For each image,

TABLE 3. Complete description of the NCC-net architecture for binary classification.

Layer	Layer type	Stride	Padding	Activations	Learnables
input	Resize	-	-	224×224×3	-
conv_1	Convolution	1×1	-	224×224×64	Weights: 7×7×3×64 Bias: 1×1×64
BN_1	Batch Normalization	-	-	224×224×64	Offset 1×1×64 Scale 1×1×64
relu_1	ReLU	-	-	224×224×64	-
conv_2	Convolution	1×1	-	224×224×64	Weights: 5×5×64×64 Bias: 1×1×64
BN_2	Batch Normalization	-	-	224×224×64	Offset 1×1×64 Scale 1×1×64
relu_2	ReLU	-	-	224×224×64	-
conv_3	Convolution	1×1	-	224×224×64	Weights: 3×3×64×64 Bias: 1×1×64
BN_3	Batch Normalization	-	-	224×224×64	Offset 1×1×64 Scale 1×1×64
relu_3	ReLU	-	-	224×224×64	-
avpool	Average pooling	2×2	0×0×0×0	112×112×64	-
relu_4	ReLU	-	-	112×112×64	-
fc	Fully Connected	-	-	1×1×2	Weights: 2×802816 Bias: 2×1
softmax	Softmax	-	-	1×1×2	-

we extracted ten patches from the region of interest (ROI) with a size of 224 × 224 pixels, obtaining a total of 14370 labeled images.

A. BINARY CLASSIFICATION

The general steps for this binary classification of cataract and non-cataract are (1) generation of patches from the slit-lamp images extracted from the ROI; (2) creation of accurate feature representations using images/patches; (3), in some cases, selection of discriminant features using principal component analysis (PCA), and (4) classification of the images into binary classes by using fully supervised classifiers. After cropping all the images and producing the training patches, feature learning is carried out by supervised deep learning. The network input is normalized with unit variance and zero mean. Rectifier linear units (ReLu) are implemented after the batch normalization layer, improving the classification accuracy and training speed instead of using the sigmoid or hyperbolic tangent functions. Fig. (6) represents the flow diagram of this scheme.

The simulations were performed with MATLAB® R2019a in a workstation with Intel® Core™ i7 1.8 GHz processor and NVIDIA GeFORCE GTX 750M GPU. The training options for the CNN were Backpropagation training with a minibatch size of 12, an initial learning rate of 0.001, and a maximum of 100 training epochs. The dataset with other images obtained from available datasets consists of 90 images; 45 are labeled as cataracts, and 45 are labeled as non-cataracts.

The experiments include the following parts: (1) applying NCC-net for feature extraction and using these features directly with SVM and ANN (NCC+ANN, and NCC+SVM), (2) applying PCA for feature selection before obtaining the feature vector used for classification with SVM and ANN (NCC+PCA+ANN, and NCC+PCA+SVM), (3) using the pre-trained networks AlexNet and GoogLeNet in transfer learning mode, training only the fully-connected layer with our images, and (5) using only our proposed NCC-net for feature extraction and classification. Some of the classification results within NCC-net are shown in Fig. 7.

The dataset consists of 70% training, 15% validation, and 15% testing sets, adopting the cross-validation technique. Each classification task uses the same dataset split without data augmentation in this work, except for patch extraction. The database increases from 90 to 900 images using patches.

In Table 4, sensitivity, specificity, accuracy, and area under the curve of ROC (AUC) are reported as evaluation metrics.

B. CLASSIFICATION OF MULTIPLE CLASSES

One of the main purposes of this research work was to obtain a considered big-enough dataset for classifying multi-level degree cataracts, aiming to compare our results with the well-known LOCS III classification system in cataracts databases. The process is similar to the binary case classification, but now classifying the images according to the LOCS III system, using cropped images, feature learning by supervised deep learning, and the same technical considerations for introducing the dataset to the classification algorithms. The training options for the CNN were Backpropagation training with a minibatch size of 12, an initial learning rate of 0.001, and a maximum of 100 training epochs. The dataset consists of 1437 labeled images; 55 labeled as NO1/NC1, 123 labeled as NO2/NC2, 112 labeled as NO3/NC3, 242 labeled as NO4/NC4, 318 labeled as NO5/NC5, and 587 labeled as NO6/NC6.

The experiments include the following parts: (1) applying NCC-net for feature extraction and using these features directly with SVM and ANN (NCC+ANN and NCC+SVM),

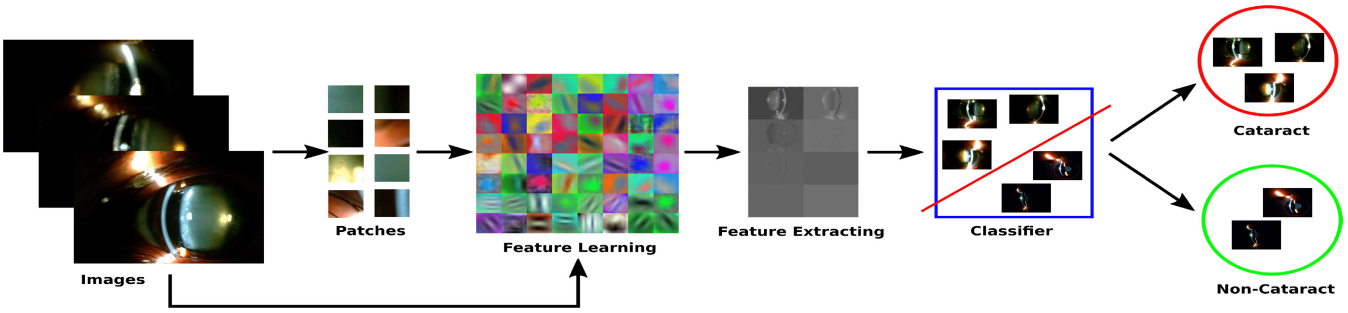

FIGURE 6. The flow diagram for the binary classification algorithms.

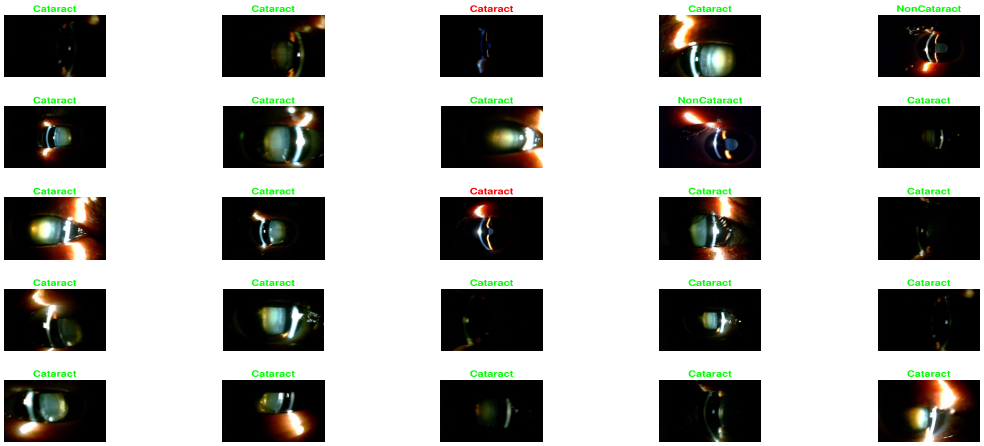

FIGURE 7. Some examples of accurate and inaccurate classified cases for both classes with the proposed NCC-net. The green ones are the corrected classified examples.

TABLE 4. Performance measures of binary classification by both traditional machine learning and CNNs including the Proposed NCC-net.

	Accuracy	Error	Sensitivity	Specificity	AUC
NCC-net	**0.9267±0.0453**	**0.0733±0.0063**	**0.9205±0.0457**	**0.9500±0.0316**	**0.9659±0.0479**
NCC+ANN	0.8639±0.0482	0.1361±0.0079	0.8940±0.0485	0.7500±0.0479	0.9363±0.0400
NCC+SVM	0.8848±0.0458	0.1152±0.0071	0.9073±0.0396	0.8000±0.0480	0.9489±0.0328
AlexNet	0.8691±0.0425	0.1309±0.0018	0.8808±0.0467	0.8250±0.0339	0.8918±0.0379
GoogLeNET	0.8901±0.0328	0.1099±0.0086	0.9073±0.0353	0.8250±0.0412	0.9518±0.0347
NCC+PCA+ANN	0.8377±0.0475	0.1623±0.0093	0.8543±0.0383	0.7750±0.0398	0.8782±0.0245
NCC+PCA+SVM	0.8482±0.0480	0.1518±0.0017	0.8609±0.0377	0.8000±0.0355	0.8873±0.0323

(2) applying PCA for feature selection before obtaining the feature vector used for classification with SVM and ANN (NCC+PCA+ANN, and NCC+PCA+SVM), (3) using the pre-trained networks AlexNet and GoogLeNet in transfer learning mode, training only the fully-connected layer with our images, and (5) using only our proposed NCC-net for feature extraction and classification. Fig. 8 presents the ROC for each method.

The dataset was split into the 70% training, 15% validation, and 15% testing sets, and the cross-validation technique was adopted. For each classification task, the same split was used. No data augmentation operation was used for this work except for patch extraction. The database was increased from 1437 to 14370 images.

In Table 5, sensitivity, specificity, accuracy, and area under the curve of ROC (AUC) are reported as evaluation metrics.

C. RASPBERRY PI IMPLEMENTATION OF THE NCC-NET

Now we analyze the implementation of NCC-net in a single board computer (SBC), a Raspberry Pi model B +. The performance should classify many images, tagged into two categories: cataract and non-cataract. After that, the algorithm and architecture adaption works without ending the board's resources. This process employs an OpenCV library with 224 × 224 pixels of pre-processed images. The dataset consists of 90 labeled images, 45 labeled as

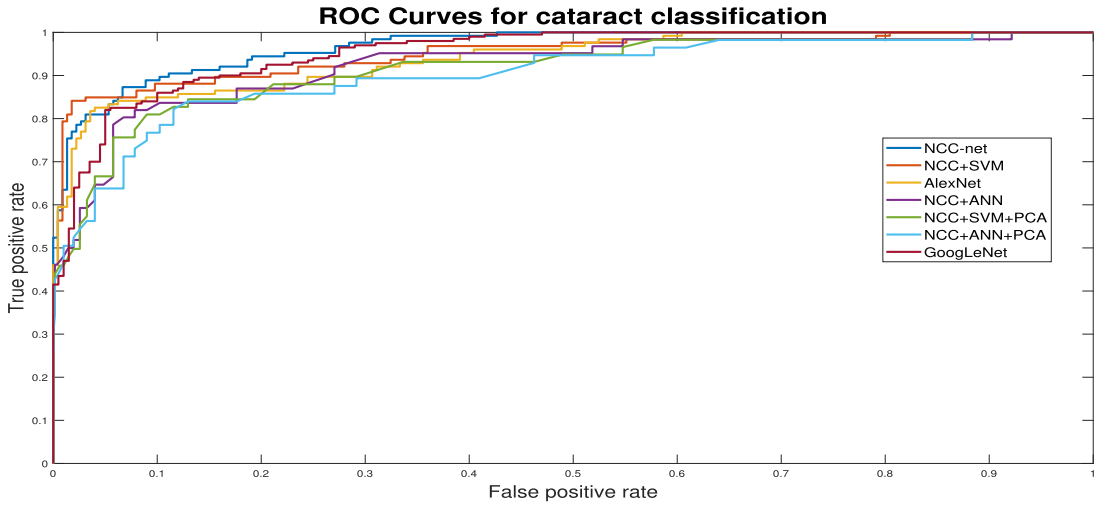

FIGURE 8. ROC Curve for all the classification methods using the LOCS III classification system.

TABLE 5. Performance measures of LOCS III classification by both traditional machine learning and CNNs including the Proposed NCC-net.

	Accuracy	Error	Sensitivity	Specificity	AUC
NCC-net	**0.8843±0.0343**	**0.1157±0.0072**	**0.9007±0.0663**	**0.9326±0.0421**	**0.8875±0.0519**
NCC+ANN	0.8331±0.0453	0.1669±0.0081	0.8743±0.0442	0.7125±0.0396	0.8321±0.0439
NCC+SVM	0.8375±0.0394	0.1625±0.0053	0.8563±0.0512	0.8412±0.0477	0.8213±0.0401
AlexNet	0.8236±0.0433	0.1764±0.0021	0.8365±0.0379	0.8021±0.0379	0.7921±0.0416
GoogLeNET	0.8301±0.0445	0.1699±0.0079	0.8563±0.0324	0.7652±0.0396	0.7833±0.0416
NCC+PCA+ANN	0.7923±0.0486	0.2077±0.0088	0.8432±0.0293	0.7750±0.0503	0.7826±0.0351
NCC+PCA+SVM	0.8024±0.0532	0.1566±0.0009	0.8609±0.0381	0.8032±0.0355	0.7963±0.0448

TABLE 6. Epoch comparison loss/accuracy value.

Epoch	loss/accuracy
5	0.48069/0.7880
10	0.6139/0.7749
50	1.3546/0.8396
100	1.8961/0.8937

TABLE 7. Specifications for the Raspberry and the training workstation.

	Raspberry PI B+	PC
CPU	ARM	i7-4500U Quadcore @1.8 GHz
RAM	512 MB	8 GB
Disk	64 GB High Speed Micro SD	256 GB SATA SSD
GPU	N/A	NVIDIA GeForce 750M
Python	3.5	3.5
OS	Raspbian	Windows 10 x64

cataracts and 45 marked as non-cataract. We extracted ten patches for each image, increasing the database ten times. The model is implemented on MATLAB® R2019a in a workstation with Intel® Core™ i7 1.8 GHz processor and NVIDIA GeForce GTX 750M GPU, and then exported to a Python model. The NCC-net model has three main layers, an input layer, a hidden layer, and an output layer. The characteristics for each layer are described in Table 3. The model was trained using gradient descent with a learning rate of 0.001, and the network was trained from 5 to 100 epochs. The results for the training can be seen in Table 6.

To test the effectiveness of implementing the architecture on the Raspberry board, 140 database images were tested. Of these 140 images, 125 were in the correct class, and 15 were in the wrong. Each image processing on the Raspberry had a different execution time. The specifications for the Raspberry and the training workstation are shown in Table 7

TABLE 8. Run test for NCC-net.

Device	i7-4500U	Raspberry Pi B+	GT 750M
Best run (ms)	4729	123221	9854
Worst run (ms)	12681	183460	31447
Average run (ms)	7747	155423	20245
Processor ussage (%)	25	100	11
Ussage/total RAM (MB)	300/8192	260/512	3800/4096

The run test is shown in Table 8 only for the NCC model. Other processes are not included in the time run result Raspberry Pi B+ can run a 3-Layer CNN, using all the resources during the simulations. The images are resized to 224 × 224 RGB. For a real-time application, greater computational power is needed to achieve classification.

V. CONCLUSION

The current tendency for massive-structure learning algorithms in artificial intelligence requires a sufficient and vast quantity of datasets for automatically extracting relevant features and classifying the disease.

The purpose of this paper follows two objectives. The first is to collaborate with a vast dataset of images for the research community working on detecting nuclear cataracts with computational-based algorithms. The dataset was obtained with the proper medical protocols and under the supervision of specialists with slit lamps from a medical center in Mexico City. The database is available online at Nuclear Cataract Database. The relevant part is the extensive dataset for comparisons on the LOCS III cataract classification system. Since the number of images is not the same for each label in the multiple degrees of disease affectation and the number of images in the database is relatively small, we employed patches of the slit-lamp images for data augmentation, increasing ten times the database size.

For the second objective, we have proposed a deep convolutional neural network called NCC-net for automatically classifying the two-degree case with only images of cataract and non-cataract and the multiple-degree case. The accuracy obtained for the binary classification using the NCC-net architecture was 93%, the sensitivity 92%, and the specificity 95%. These performance values were higher than the transfer learning mode and fine-tuning of known deep architectures like the GoogLeNET network with 89% of accuracy. In the same way, we implemented this network in an embedded system called Raspberry Pi B+, showing very competitive results. The accuracy achieved after 50 training epochs was 84%, while for 100 epochs, the accuracy raised to 89%. The simulation time for the Raspberry Pi B + also shows promising results. While for a workstation, the worst simulation time was 12 seconds; the simulation time was approximately 3.5 minutes for the Raspberry. Finally, we present a multiple-level disease classification according to the LOCS III classification. We demonstrated that our system has performance indicators for a reliable pre-diagnosis based on medical expertise for this multi-class task and the enlarged database. The accuracy obtained was 88%, the sensitivity 90%, and the specificity 93%, higher values than those obtained with the proposed experiments and fine-tuned deep architectures; that is, the NCC+ANN framework with 83% of accuracy for the multi-class.

The patients may have other diseases interfering with the cataract features in slit-lamp images. We cannot distinguish these diseases from cataracts; therefore, further research should focus on improving this. With high-order features extracted for cataract classification, the proposed CNN allows an automated pre-diagnosis of nuclear cataracts in slit-lamp images. Finally, we can conclude that this algorithm can help to carry out the first examination step for a proper medical diagnosis.

REFERENCES

[1] J. Bajwa, U. Munir, A. Nori, and B. Williams, "Artificial intelligence in healthcare: Transforming the practice of medicine," *Future Healthcare J.*, vol. 8, no. 2, p. e188, 2021.

[2] A. Rajkomar, J. Dean, and I. Kohane, "Machine learning in medicine," *New England J. Med.*, vol. 380, no. 14, pp. 1347–1358, 2019.

[3] A. Alwosheel, S. van Cranenburgh, and C. G. Chorus, "Is your dataset big enough? Sample size requirements when using artificial neural networks for discrete choice analysis," *J. Choice Model.*, vol. 28, pp. 167–182, Sep. 2018.

[4] A. McDonald, "Data quality considerations for petrophysical machine-learning models," *Petrophysics*, vol. 62, no. 6, pp. 585–613, 2021.

[5] H. Kirkpatrick, "The etiology of primary cataract," *British Med. J.*, vol. 1, no. 3195, p. 467, 1922.

[6] R. A. Ramlee, A. R. Ramli, and H. A. Sulaiman, "A review on diseases manifestation by ocular diseases using computer aided diagnosis (CAD)," *Int. J. Eng. Technol.*, vol. 7, no. 4, pp. 1343–1348, 2015.

[7] *World Report on Vision*, World Health Organization, Geneva, Switzerland, 2019.

[8] R. Supriyanti, H. Habe, M. Kidode, and S. Nagata, "Compact cataract screening system: Design and practical data acquisition," in *Proc. Int. Conf. Instrum., Commun., Inf. Technol., Biomed. Eng.*, Nov. 2009, pp. 1–6.

[9] S. G. Kachewar and D. S. Kulkarni, "An imaging review of intra-ocular calcifications," *J. Clin. Diagnostic Res.*, vol. 8, no. 1, pp. 203–205, 2014.

[10] A. B. Hall, J. R. Thompson, J. S. Deane, and A. R. Rosenthal, "LOCS III versus the Oxford Clinical Cataract Classification and Grading System for the assessment of nuclear, cortical and posterior subcapsular cataract," *Ophthalmic Epidemiol.*, vol. 4, no. 4, pp. 179–194, 1997.

[11] L. T. Chylack Jr., M. C. Leske, D. McCarthy, P. Khu, T. Kashiwagi, and R. Sperduto, "Lens opacities classification system II (LOCS II)," *Archives Ophthalmol.*, vol. 107, no. 7, pp. 991–997, 1989.

[12] J. M. Sparrow, A. J. Bron, N. A. P. Brown, W. Ayliffe, and A. R. Hill, "The Oxford clinical cataract classification and grading system," *Int. Ophthalmol.*, vol. 9, no. 4, pp. 207–225, Dec. 1986.

[13] L. T. Chylack Jr., J. K. Wolfe, D. M. Singer, M. C. Leske, M. A. Bullimore, I. L. Bailey, J. Friend, D. McCarthy, and S. Y. Wu, "The lens opacities classification system III," *Archives Ophthalmol.*, vol. 111, no. 6, pp. 831–836, 1993.

[14] X.-Q. Zhang, Y. Hu, Z.-J. Xiao, J.-S. Fang, R. Higashita, and J. Liu, "Machine learning for cataract classification/grading on ophthalmic imaging modalities: A survey," *Mach. Intell. Res.*, vol. 19, no. 3, pp. 184–208, 2022.

[15] A. W. P. Foong, S.-M. Saw, J.-L. Loo, S. Shen, S.-C. Loon, M. Rosman, T. Aung, D. T. H. Tan, E. S. Tai, and T. Y. Wong, "Rationale and methodology for a population-based study of eye diseases in Malay people: The Singapore Malay eye study (SiMES)," *Ophthal. Epidemiol.*, vol. 14, no. 1, pp. 25–35, 2007, doi: 10.1080/09286580600878844.

[16] J. Liu, D. W. K. Wong, Z. Zhang, B.-H. Lee, X. Gao, F. Yin, J. Zhang, and M. T. Htoo, "Integrating research, clinical practice and translation: The Singapore experience," in *Proc. 35th Annu. Int. Conf. IEEE Eng. Med. Biol. Soc. (EMBC)*, Jul. 2013, pp. 7148–7151.

[17] J. Jiang, S. Lei, M. Zhu, R. Li, J. Yue, J. Chen, Z. Li, J. Gong, D. Lin, X. Wu, Z. Lin, and H. Lin, "Improving the generalizability of infantile cataracts detection via deep learning-based lens partition strategy and multicenter datasets," *Frontiers Med.*, vol 8, May 2021, Art. no. 664023.

[18] J. Cuadros and G. Bresnick, "EyePACS: An adaptable telemedicine system for diabetic retinopathy screening," *J. Diabetes Sci. Technol.*, vol. 3, pp. 509–516, May 2009.

[19] A. D. Hoover, V. Kouznetsova, and M. Goldbaum, "Locating blood vessels in retinal images by piecewise threshold probing of a matched filter response," *IEEE Trans. Med. Imag.*, vol. 19, no. 3, pp. 203–210, Mar. 2000.

[20] T. Kauppi, V. Kalesnykiene, J.-K. Kamarainen, L. Lensu, I. Sorri, H. Uusitalo, H. Kälviäinen, and J. Pietilä, "DIARETDB0: Evaluation database and methodology for diabetic retinopathy algorithms," Mach. Vis. Pattern Recognit. Res. Group, Lappeenranta Univ. Technol., Lappeenranta, Finland, Tech. Rep. 73, 2006, pp. 1–17.

[21] E. Decencière, X. Zhang, G. Cazuguel, B. Lay, B. Cochener, C. Trone, P. Gain, R. Ordonez, P. Massin, A. Erginay, B. Charton, and J.-C. Klein, "Feedback on a publicly distributed image database: The Messidor database," *Image Anal. Stereol.*, vol. 33, no. 3, pp. 231–234, 2014.

[22] J. Staal, M. D. Abramoff, M. Niemeijer, M. A. Viergever, and B. van Ginneken, "Ridge-based vessel segmentation in color images of the retina," *IEEE Trans. Med. Imag.*, vol. 23, no. 4, pp. 501–509, Apr. 2004.

[23] E. J. Carmona, M. Rincón, J. García-Feijoó, and J. M. Martínez-de-la-Casa, "Identification of the optic nerve head with genetic algorithms," *Artif. Intell. Med.*, vol. 43, no. 3, pp. 243–259, 2008.

[24] P. Porwal, S. Pachade, R. Kamble, M. Kokare, G. Deshmukh, V. Sahasrabuddhe, and F. Meriaudeau, "Indian diabetic retinopathy image dataset (IDRiD): A database for diabetic retinopathy screening research," *Data*, vol. 3, no. 4, p. 25, Jul. 2018.

[25] X. Gao, D. W. K. Wong, A. W. Aryaputera, Y. Sun, C.-Y. Cheng, C. Cheung, and T. Y. Wong, "Automatic pterygium detection on cornea images to enhance computer-aided cortical cataract grading system," in *Proc. Annu. Int. Conf. IEEE Eng. Med. Biol. Soc.*, Sep. 2012, pp. 4434–4437.

[26] D. Marina, M. E. Gegundez-Ariasb, A. Sueroa, and J. M. Bravo, "Obtaining optic disc center and pixel region by automatic thresholding methods on morphologically processed fundus images," *Comput. Programs Methods Biomed.*, vol. 118, pp. 173–185, Dec. 2014.

[27] H. Li, X. Gao, M. H. Tan, Y. C. Chow, J. H. Lim, Y. Sun, C. C. Cheung, and T. Y. Wong, "Lens image registration for cataract detection," in *Proc. 6th IEEE Conf. Ind. Electron. Appl.*, Jun. 2011, pp. 132–135.

[28] H. Li, J. H. Lim, J. Liu, and T. Y. Wong, "Towards automatic grading of nuclear cataract," in *Proc. 29th Annu. Int. Conf. IEEE Eng. Med. Biol. Soc.*, Aug. 2007, pp. 4961–4964.

[29] H. Li, J. H. Lim, J. Liu, P. Mitchell, A. G. Tan, J. J. Wang, and T. Y. Wong, "A computer-aided diagnosis system of nuclear cataract," *IEEE Trans. Biomed. Eng.*, vol. 57, no. 7, pp. 1690–1698, Jul. 2010.

[30] H. Li, J. H. Lim, J. Liu, D. W. K. Wong, N. M. Tan, S. Lu, Z. Zhang, and T. Y. Wong, "Computerized systems for cataract grading," in *Proc. 2nd Int. Conf. Biomed. Eng. Informat.*, Oct. 2009, pp. 1–4.

[31] K. R. Salla and S. S. Kadam, "A fuzzy inference system based approach for detection, classification and grading of cataract," *Int. J. Comput. Sci. Appl. Issue*, vol. 47, pp. 18–23, 2010.

[32] R. U. Acharya, W. Yu, K. Zhu, J. Nayak, T.-C. Lim, and J. Y. Chan, "Identification of cataract and post-cataract surgery optical images using artificial intelligence techniques," *J. Med. Syst.*, vol. 34, no. 4, pp. 619–628, 2010.

[33] W. Huang, K. L. Chan, H. Li, J. H. Lim, J. Liu, and T. Y. Wong, "A computer assisted method for nuclear cataract grading from slit-lamp images using ranking," *IEEE Trans. Med. Imag.*, vol. 30, no. 1, pp. 94–107, Jan. 2011, doi: 10.1109/TMI.2010.2062197.

[34] M. Yang, J.-J. Yang, Q. Zhang, Y. Niu, and J. Li, "Classification of retinal image for automatic cataract detection," in *Proc. IEEE 15th Int. Conf. E-Health Netw., Appl. Services (Healthcom)*, Oct. 2013, pp. 674–679.

[35] X. Gao, S. Lin, and T. Y. Wong, "Automatic feature learning to grade nuclear cataracts based on deep learning," *IEEE Trans. Biomed. Eng.*, vol. 62, no. 11, pp. 2693–2701, Nov. 2015.

[36] L. Guo, J.-J. Yang, L. Peng, J. Li, and Q. Liang, "A computer-aided healthcare system for cataract classification and grading based on fundus image analysis," *Comput. Ind.*, vol. 69, pp. 72–80, May 2015.

[37] L. Xiong, H. Li, and L. Xu, "An approach to evaluate blurriness in retinal images with vitreous opacity for cataract diagnosis," *J. Healthcare Eng.*, vol. 2017, Apr. 2017, Art. no. 5645498.

[38] X. Xu, L. Zhang, J. Li, Y. Guan, and L. Zhang, "A hybrid global–local representation CNN model for automatic cataract grading," *IEEE J. Biomed. Health Informat.*, vol. 24, no. 2, pp. 556–567, Feb. 2020.

[39] M. S. Junayed, M. B. Islam, A. Sadeghzadeh, and S. Rahman, "CataractNet: An automated cataract detection system using deep learning for fundus images," *IEEE Access*, vol. 9, pp. 128799–128808, 2021.

[40] M. S. M. Khan, M. Ahmed, R. Z. Rasel, and M. M. Khan, "Cataract detection using convolutional neural network with VGG-19 model," in *Proc. IEEE World AI IoT Congr. (AIIoT)*, May 2021, pp. 0209–0212.

[41] M. Rajib Hossain, S. Afroze, N. Siddique, and M. Moshiul Hoque, "Automatic detection of eye cataract using deep convolution neural networks (DCNNs)," in *Proc. IEEE Region 10 Symp. (TENSYMP)*, Jun. 2020, pp. 1333–1338.

[42] A. A. Bhadra, M. Jain, and S. Shidnal, "Automated detection of eye diseases," in *Proc. Int. Conf. Wireless Commun., Signal Process. Netw. (WiSPNET)*, Mar. 2016, pp. 1341–1345.

[43] S. Pathak and B. Kumar, "A robust automated cataract detection algorithm using diagnostic opinion based parameter thresholding for telemedicine application," *Electronics*, vol. 5, no. 3, p. 57, Sep. 2016.

[44] A. B. Jagadale and D. V. Jadhav, "Early detection and categorization of cataract using slit-lamp images by Hough circular transform," in *Proc. Int. Conf. Commun. Signal Process. (ICCSP)*, Apr. 2016, pp. 232–235.

[45] V. F. Pamplona, E. B. Passos, J. Zizka, M. M. Oliveira, E. Lawson, E. Clua, and R. Raskar, "CATRA: Interactive measuring and modeling of cataracts," in *Proc. ACM Trans. Graph. (TOG)*, vol. 30, 2011, p. 47.

[46] W. Huang, H. Li, K. L. Chan, J. H. Lim, J. Liu, and T. Y. Wong, "A computer-aided diagnosis system of nuclear cataract via ranking," in *Proc. Int. Conf. Med. Image Comput. Comput.-Assist. Intervent.* Berlin, Germany: Springer, 2009, pp. 803–810.

[47] J. G. Greener, S. M. Kandathil, L. Moffat, and D. T. Jones, "A guide to machine learning for biologists," *Nature Reviews Mol. Cell Biol.*, vol. 23, no. 1, pp. 40–55, 2022.

[48] T. Hastie, R. Tibshirani, and J. Friedman, *The Elements of Statistical Learning: Data Mining, Inference, and Prediction*, vol. 2. New York, NY, USA: Springer, 2009.

[49] W. Liu, Z. Wang, X. Liu, N. Zeng, Y. Liu, and F. E. Alsaadi, "A survey of deep neural network architectures and their applications," *Neurocomputing*, vol. 234, pp. 11–26, Apr. 2017.

[50] H. Zhang, K. Niu, Y. Xiong, W. Yang, Z. He, and H. Song, "Automatic cataract grading methods based on deep learning," *Comput. Methods Programs Biomed.*, vol. 182, Dec. 2019, Art. no. 104978.

[51] B. K. Desai, "Slit lamp examination," in *Atlas of Emergency Medicine Procedures*, L. Ganti, Ed. New York, NY, USA: Springer, 2016, doi: 10.1007/978-1-4939-2507-0_46.

[52] I. P. U. Breton and V. L. Gómez, "Opacidad del cristalino de acuerdo al sistema LOCS III en una muestra hospitalaria mexicana," *Revista Hospital Juárez México*, vol. 77, no. 1, pp. 43–49, 2010.

[53] I. Cruz-Vega and H. I. Morales, 2023, "Nuclear cataract database for biomedical and machine learning applications," *Mendeley Data*, Version 2, doi: 10.17632/6wv33nbcvv.2.

[54] D. Kim, T. J. Jun, Y. Eom, C. Kim, and D. Kim, "Tournament based ranking CNN for the cataract grading," in *Proc. 41st Annu. Int. Conf. IEEE Eng. Med. Biol. Soc. (EMBC)*, Jul. 2019, pp. 1630–1636.

[55] H. Li, L. Ko, J. H. Lim, J. Liu, D. W. K. Wong, T. Y. Wong, and Y. Sun, "Automatic opacity detection in retro-illumination images for cortical cataract diagnosis," in *Proc. IEEE Int. Conf. Multimedia Expo*, Apr. 2008, pp. 553–556.

[56] H. Li, L. Ko, J. H. Lim, J. Liu, D. W. K. Wong, and T. Y. Wong, "Image based diagnosis of cortical cataract," in *Proc. 30th Annu. Int. Conf. IEEE Eng. Med. Biol. Soc.*, Aug. 2008, pp. 3904–3907.

[57] H. Li, J. H. Lim, J. Liu, D. W. K. Wong, and T. Y. Wong, "Computer aided diagnosis of nuclear cataract," in *Proc. 3rd IEEE Conf. Ind. Electron. Appl.*, Jun. 2008, pp. 1841–1844.

[58] H. Li, J. H. Lim, J. Liu, D. W. K. Wong, N. M. Tan, S. Lu, Z. Zhang, and T. Y. Wong, "An automatic diagnosis system of nuclear cataract using slit-lamp images," in *Proc. Annu. Int. Conf. IEEE Eng. Med. Biol. Soc.*, Sep. 2009, pp. 3693–3696.

[59] H. Li, J. H. Lim, J. Liu, D. W. K. Wong, Y. Foo, Y. Sun, and T. Y. Wong, "Automatic detection of posterior subcapsular cataract opacity for cataract screening," in *Proc. Annu. Int. Conf. IEEE Eng. Med. Biol.*, Sep. 2010, pp. 5359–5362.

[60] X. Gao, H. Li, J. H. Lim, and T. Y. Wong, "Computer-aided cataract detection using enhanced texture features on retro-illumination lens images," in *Proc. 18th IEEE Int. Conf. Image Process.*, Sep. 2011, pp. 1565–1568.

[61] W. Song, P. Wang, X. Zhang, and Q. Wang, "Semi-supervised learning based on cataract classification and grading," in *Proc. 40th Annu. Comput. Softw. Appl. Conf. (COMPSAC)*, Jun. 2016, pp. 641–646.

[62] H. I. Morales-Lopez, I. Cruz-Vega, J. M. Ramirez-Cortes, H. Peregrina-Barreto, and J. Rangel-Magdaleno, "SOM-like neural network and differential evolution for multi-level image segmentation and classification in slit-lamp images," in *Proc. IEEE Colombian Conf. Appl. Comput. Intell.* Cham, Switzerland: Springer, 2018, pp. 26–37.

[63] S. Hu, X. Wang, H. Wu, X. Luan, P. Qi, Y. Lin, X. He, and W. He, "Unified diagnosis framework for automated nuclear cataract grading based on smartphone slit-lamp images," *IEEE Access*, vol. 8, pp. 174169–174178, 2020.

[64] T. Tasin and M. A. Habib, "Computer-aided cataract detection using random forest classifier," in *Proc. Int. Conf. Big Data, IoT, Mach. Learn.* Singapore: Springer, 2022, pp. 27–38.
[65] S. A. Hick, I. Strümke, V. Thambawita, M. Hammou, M. A. Riegler, P. Halvorsen, and S. Parasa, "On evaluation metrics for medical applications of artificial intelligence," *Sci. Rep.*, vol. 12, no. 1, pp. 1–9, 2022.

ISRAEL CRUZ-VEGA received the B.Sc. degree from the National Polytechnic Institute, Mexico, and the M.Sc. and Ph.D. degrees in automatic control from the Center of Research and Advances Studies (CINVESTAV), Mexico. He holds a research position as a CONACYT-Research Fellow of the Electronics Department, National Institute of Astrophysics, Optics, and Electronics (INAOE). He is also a member of the Mexican National Research System (SNI), level 1. His research interests include control theory, drone control, chaos prediction, and the applications of computational intelligence.

HANS ISRAEL MORALES-LOPEZ received the B.Sc. degree from Beneremerita Universidad Autonoma de Puebla (BUAP), and the M.Sc. and Ph.D. degrees in electronics specialization from the National Institute of Astrophysics, Optics, and Electronics (INAOE). His research interests include machine learning and embedded electronics.

JUAN MANUEL RAMIREZ-CORTES (Senior Member, IEEE) received the B.Sc. degree in electrical engineering from the National Polytechnic Institute, Mexico, the M.Sc. degree in electrical engineering from the National Institute of Astrophysics, Optics, and Electronics (INAOE), Mexico, and the Ph.D. degree in electrical engineering from Texas Tech University. He is currently a Researcher with the Electronics Department, INAOE. He is also a member of the Mexican National Research System (SNI), level 2. His research interests include signal and image processing, biometrics, neural networks, fuzzy logic, and digital systems.

JOSE DE JESUS RANGEL-MAGDALENO (Senior Member, IEEE) received the B.E. degree in electronics engineering and the M.E. degree in electrical engineering on hardware signal processing from Universidad de Guanajuato, Mexico, in 2006 and 2008, respectively, and the Ph.D. degree from Universidad Autonoma de Queretaro, Mexico, in 2011. He is currently a Tenured Researcher with the Electronics Department, National Institute of Astrophysics, Optics, and Electronics (INAOE), Mexico. He has authored one book and over 140 works published in book chapters, journals, and conferences. His research interests include FPGAs, signal and image processing, and instrumentation. He is a member of the Mexican National Research System (SNI), Level 2. He received the 2018 IEEE I&MS Outstanding Young Engineer Award.